Regular paper

Multifrequency microwave thermograph for biomedical applications

Bronisław Stec, Andrzej Dobrowolski, and Waldemar Susek

Abstract — This paper presents problems related to thermal radiation of human bodies in microwave range in aspect of diagnosis of breast carcinoma. A mathematical model of thermal radiation transfer through tissues is introduced and methods of measurement of temperature, depth and size of a heat source, by means of multifrequency microwave thermography are described. Theoretical considerations are supplemented by presentation of experimental results.

Keywords — microwave thermograph, radiometer, thermal radiation, breast carcinoma.

1. Introduction

The passive microwave thermography is based on measurement of thermal radiation emitted by each body, which has the temperature higher than the absolute zero [1–8]. The greatest intensity of radiation is in the infrared, but high attenuation of tissue in this range limits application of the infrared thermography to measurements of skin temperature only. In the microwave frequency range the intensity of radiation is about ten million times lower but attenuation of tissue is low, too. Moreover in this range the intensity of radiation is directly proportional to absolute temperature.

Thermal radiation from a biological body is attenuated by each layer of tissue. Moreover it is reflected and at the same time refracted on the interfaces between different layers [9]. The initial analysis indicates that attenuation, characterised by depth of penetration, is the most important factor.

Analysis of characteristics of radiation and attenuation makes it possible to conclude, that measurements on several frequencies will enable us to estimate the depth and size of the heat source [10–14]. Computer simulation shows that for anatomical depths of the heat source, the maximum intensity of the received radiation is in the frequency range between 1 GHz and 5 GHz. Therefore, we use radiometers working in this range.

In microwave radiometers temperature measurement is made essentially by measuring the thermal noise power [15]. Considering the method of thermal noise power measurement, microwave radiometers can be divided into two groups: total power (compensatory) radiometers and modulation radiometers (Dicke radiometers). Modulation radiometers can be further divided into self-balancing ones and those with compensation of reflection coefficient.

In Dicke radiometers, the output signal carrying information about temperature difference is directly proportional to the gain of high frequency section. This requires high stability and periodical calibration with reference noise source. It is also important that temperature reading depends not only on temperature of examined tissues but also on imperfect matching between antenna and measured object. As a result, Dicke radiometers have to be recalibrated before every single measurement, which is very strenuous in clinical applications.

Using self-balancing radiometer with internal, controlled noise source can eliminate errors resulting from gain changes. Block diagram of such a device with additional compensation of reflection coefficient of antenna-tissue interface is presented in [16]. In such radiometer, the input power is compared with power from internal noise source. As a result of self-balancing procedure voltage at the output of low-pass filter goes to zero. Thus the result of measurement is independent from radiometer's gain.

In previous designs of radiometers constructed in Military University of Technology in Warsaw internal noise source was controlled by analogue regulation loop. Error signal from the output of synchronous detector was transmitted to regulation elements of internal noise generator, which were nonlinear PIN diodes. To ensure quasi-linear conversion characteristics of radiometer, the temperature range had to be limited.

Limitation mentioned above can be successfully overcome using computer-controlled digital regulation loop [17] presented in Fig. 1. Regulation voltage of the internal noise generator changes until zero output voltage is reached. Temperature is calculated by software, which takes into account effects nonlinear characteristics of regulation elements.

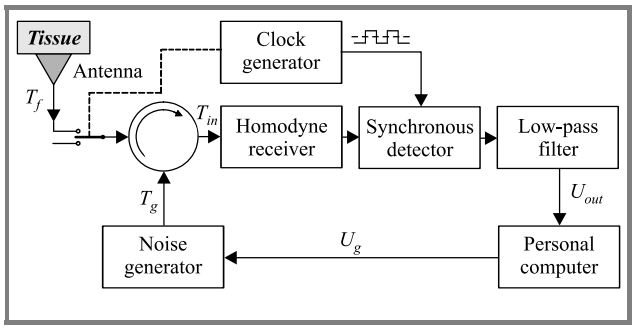

Fig. 1. Block diagram of a radiometer with compensation of reflection coefficient and digitally controlled internal noise source.

Application of optimal control and conversion algorithm reduced the sensitivity of temperature measurement to changes of environmental parameters such as electrical properties and ambient temperature. A homodyne receiver

was used in measurement unit described above, which reduces noise level and improves temperature resolution. Further performance improvement is obtained by fully digital synchronous detection and low-pass filtering by digital signal processor.

Monofrequency radiometry enables measurement of average temperature of a certain area. Therefore, we do not know whether the heat source is cool and just under the skin or perhaps it is hot, but deeply located. In both cases the thermal brightness of the external surface may be equal. This is illustrated in Fig. 2. We only know that there is an area of increased temperature under the antenna, which may indicate the presence of tumour.

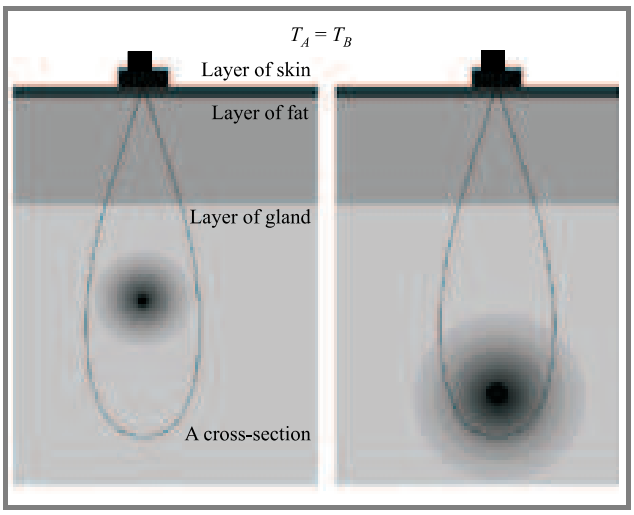

Fig. 2. Monofrequency microwave thermography.

Estimation of spatial temperature distribution inside the investigated object is particularly interesting from the practical point of view. The solution presented below uses the power thermography at different frequencies [18, 19]. This method is based on increase of intensity of thermal radiation and decrease of penetration depth into biological tissues with frequency.

Spatial temperature distribution can be determined by measurements taken in adjacent points. Therefore in next chapters the uni-dimensional analysis of deep-seated profile of temperature distribution will be presented as well as algorithm of inverse transformation converting the results of multiband measurements of temperature brightness on the external surface into deep-seated temperature distribution.

2. Temperature brightness of the external surface

As presented in [20, 21] three-layer model of tissue, increase of physical temperature of the internal heat source T results in increase of the temperature brightness T' of the external surface of tissue in accordance with the following formula

$$T' = T\,\mathrm{e}^{-\frac{d_g}{\delta_g}} t_{gf}\,\mathrm{e}^{-\frac{d_f}{\delta_f}} t_{fs}\,\mathrm{e}^{-\frac{d_s}{\delta_s}}, \tag{1}$$

where: d_g, d_f, d_s – distances in gland, fat and skin layers; δ_g, δ_f, δ_s – power penetration depths in each layer; t_{gf}, t_{fs} – coefficients of power transmission at layer interfaces.

Moreover, increase of the temperature brightness T_f measured by a radiometer working at frequency f depends on reflection coefficient of the antenna – skin interface Γ_f and can be described as follows

$$T_f = T'\left(1 - \left|\Gamma_f\right|^2\right) K_T = T' K_f, \tag{2}$$

where: K_T – a factor defined as displayed temperature increase/real temperature increase ratio; K_f – a resultant coefficient included – moreover – actual antenna – tissue matching.

In medicine, particularly in oncology, there is no point source of heat but unknown temperature distribution $T(z)$. The authors aim at finding $T(z)$ distribution on the basis of discrete measurements of T_{fi} values. This typical problem has no unique solution. Analysis of this problem shows that in order to obtain estimate solution it is necessary to take some simplifying assumptions regarding the source of thermal radiation and type of estimated temperature distribution.

From the structure of tissue and properties of an initial stage of a tumour [22, 23], one can conclude that cancer has a spherical shape and the distribution of temperature originating from it exponentially decreases to zero in the layer of gland. Therefore, the Gauss curve has been assumed as the fitting function for deep-seated temperature distribution:

$$T(z) = T_S\,\mathrm{e}^{-\left(\frac{z-d_g}{\sigma}\right)^2}. \tag{3}$$

This is illustrated in Fig. 3. In this situation, increase of physical temperature of the internal heat source causes increase of temperature brightness of the external surface T_f, and is expressed by the following equation:

$$T_f = T_g\, t_{gf}\,\mathrm{e}^{-\frac{d_f}{\delta_f}} t_{fs}\,\mathrm{e}^{-\frac{d_s}{\delta_s}} K_f. \tag{4}$$

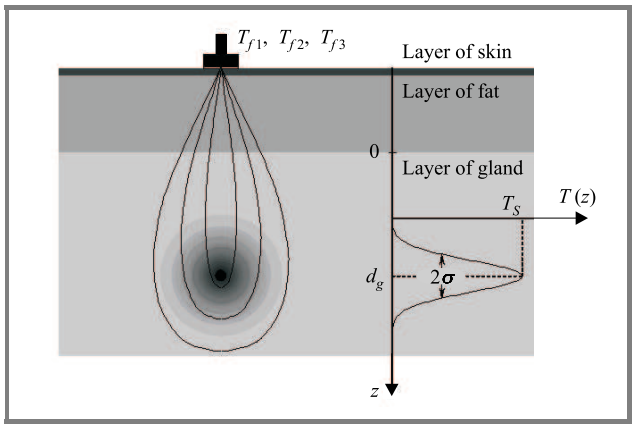

Fig. 3. Distribution of temperature inside biological tissue.

In this equation T_g is the effective temperature on the gland – fat interface and it is defined by integral of temperature distribution $T(z)$ in a range from zero to infinity, with regard to transfer coefficient:

$$\xi(z) = \mathrm{e}^{-\frac{z}{\delta_g}}. \tag{5}$$

From Eqs. (3) and (5) we obtain:

$$T(\xi) = T_S \mathrm{e}^{-\left(\frac{d_g}{\sigma}\right)^2} \xi^{-\frac{\delta_g}{\sigma^2}\left(\delta_g \ln \xi + 2d_g\right)}. \tag{6}$$

Integrating in relation to z from zero to infinity is equivalent to integrating in relation to ξ from zero to one, and consequently the temperature brightness on the gland – fat interface can be written as

$$T_g = \int_0^1 T(\xi)\mathrm{d}\xi. \tag{7}$$

Unfortunately there is no expression, which describes antiderivative of a function shown above, but it is possible to derive a formula for a definite integral as follows:

$$T_g = \frac{T_S \sigma\sqrt{\pi}}{2\delta_g} \mathrm{e}^{\frac{\sigma^2 - 4\delta_g d_g}{4\delta_g^2}} \left[\mathrm{erf}\left(\frac{2\delta_g d_g - \sigma^2}{2\delta_g \sigma}\right) + 1\right]. \tag{8}$$

As according to the initial assumptions, the following relationship is valid across analysed spectral range (1.5–4.4 GHz):

$$\mathrm{erf}\left(\frac{2\delta_g d_g - \sigma^2}{2\delta_g \sigma}\right) \approx 1 \tag{9}$$

and Eq. (8) simplifies to

$$T_g = \frac{T_S \sigma\sqrt{\pi}}{\delta_g} \mathrm{e}^{\frac{\sigma^2 - 4\delta_g d_g}{4\delta_g^2}}. \tag{10}$$

Substituting Eq. (10) into Eq. (4), we obtain the following formula:

$$T_f = \frac{T_S \sigma\sqrt{\pi}}{\delta_g} \mathrm{e}^{\frac{\sigma^2 - 4\delta_g d_g}{4\delta_g^2}} t_{gf} \mathrm{e}^{-\frac{d_f}{\delta_f}} t_{fs} \mathrm{e}^{-\frac{d_s}{\delta_s}} K_f. \tag{11}$$

This formula defines relationship between increase of the physical temperature of the internal heat source and increase of temperature brightness on the external surface measured by a radiometer operating at frequency f.

3. The inverse transformation

3.1. The homogeneous layer of tissue

In case of a single muscle layer, formula (11), which describes temperature brightness of the external surface, measured at frequency f_i as a function of deep-seated temperature distribution can be expressed as

$$T_{fi} = \frac{T_s \sigma\sqrt{\pi}}{\delta_{mi}} \mathrm{e}^{\frac{\sigma^2 - 4\delta_{mi} d_m}{4\delta_{mi}^2}} K_{fi}. \tag{12}$$

As a result of a calibration process we obtained coefficients K_{fi} $(i = 1,2,3)$ for three radiometers working at different frequencies. Using these coefficients and proper power penetration depths δ_{mi} we can estimate the real temperature distribution by means of multifrequency measurement.
By solving the set consisting of Eq. (12) for three frequencies (f_1, f_2, f_3):

$$\begin{cases} T_{f1} = \dfrac{T_s \sigma\sqrt{\pi}}{\delta_{m1}} \mathrm{e}^{\frac{\sigma^2 - 4\delta_{m1} d_m}{4\delta_{m1}^2}} K_{f1}, \\ T_{f2} = \dfrac{T_s \sigma\sqrt{\pi}}{\delta_{m2}} \mathrm{e}^{\frac{\sigma^2 - 4\delta_{m2} d_m}{4\delta_{m2}^2}} K_{f2}, \\ T_{f3} = \dfrac{T_s \sigma\sqrt{\pi}}{\delta_{m3}} \mathrm{e}^{\frac{\sigma^2 - 4\delta_{m3} d_m}{4\delta_{m3}^2}} K_{f3}, \end{cases} \tag{13}$$

we obtain expressions describing the real temperature distribution inside investigated tissue:

$$\begin{gathered} d_m = \frac{\alpha \cdot \delta_{m1}^2\left(\delta_{m2}^2 - \delta_{m3}^2\right) - \beta \cdot \delta_{m3}^2\left(\delta_{m1}^2 - \delta_{m2}^2\right)}{\delta_{m1}^2(\delta_{m2} - \delta_{m3}) - \delta_{m2}^2(\delta_{m1} - \delta_{m3}) + \delta_{m3}^2(\delta_{m1} - \delta_{m2})}, \\ \sigma = 2\delta_{m1}\delta_{m2}\sqrt{\frac{d_m\left(\delta_{m2}^{-1} - \delta_{m1}^{-1}\right) - \alpha}{\delta_{m1}^2 - \delta_{m2}^2}}, \\ T_S = \frac{T_{f1}\delta_{m1}}{\sigma K_{f1}\sqrt{\pi}} \mathrm{e}^{\frac{4\delta_{m1} d_m - \sigma^2}{4\delta_{m1}^2}}, \end{gathered} \tag{14}$$

where:

$$\alpha = \ln\left(\frac{T_{f1} K_{f2} \delta_{m1}}{T_{f2} K_{f1} \delta_{m2}}\right), \quad \beta = \ln\left(\frac{T_{f2} K_{f3} \delta_{m2}}{T_{f3} K_{f2} \delta_{m3}}\right).$$

The equations presented above were used for experimental verification of described method used to estimate the temperature, depth and size of an internal heat source, by means of multifrequency microwave thermograph.

3.2. The tissue consist of gland, fat and skin layers

When the measured tissue consists of separate layers of gland, fat and skin it is necessary to perform four-band measurement. In this case, formula (11), which describes temperature brightness on the external surface, measured at frequency f_i as a function of deep-seated temperature distribution can be written as

$$T_{fi} = \frac{T_S \sigma\sqrt{\pi}}{\delta_{gi}} \mathrm{e}^{\frac{\sigma^2 - 4\delta_{gi} d_g}{4\delta_{gi}^2}} t_{gfi} \mathrm{e}^{-\frac{d_f}{\delta_{fi}}} t_{fsi} \mathrm{e}^{-\frac{d_s}{\delta_{si}}} K_{fi}. \tag{15}$$

The layer of skin in tested place, taking into account its thickness, can be treated as a thin layer. Consequently, Eq. (15) assumes the following form:

$$T_{fi} = \frac{T_S \sigma\sqrt{\pi}}{\delta_{gi}} \mathrm{e}^{\frac{\sigma^2 - 4\delta_{gi} d_g}{4\delta_{gi}^2}} t_{gfi} \mathrm{e}^{-\frac{d_f}{\delta_{fi}}} K_{fi}. \tag{16}$$

Based on the Fresnel's formulas and using dielectric data of tissues from [24], coefficient of power transmission on the gland and fat interface t_{gfi} is about 0.96 across analysed spectral range and for an angle of incidence within $\pm 25^\circ$. As a consequence, formula (16) can be expressed as:

$$T_{fi} = \frac{T_S \sigma \sqrt{\pi}}{\delta_{gi}} \mathrm{e}^{\frac{\sigma^2 - 4\delta_{gi} d_g}{4\delta_{gi}^2}} \mathrm{e}^{-\frac{d_f}{\delta_{fi}}} 0.96 K_{fi} . \tag{17}$$

Conducting four-band measurement using four radiometers and applying formula (17), the following set of nonlinear equations is obtained:

$$\begin{cases} T_{f1} = \dfrac{T_S \sigma \sqrt{\pi}}{\delta_{g1}} \mathrm{e}^{\frac{\sigma^2 - 4\delta_{g1} d_g}{4\delta_{g1}^2}} \mathrm{e}^{-\frac{d_f}{\delta_{f1}}} 0.96 K_{f1} \\ T_{f2} = \dfrac{T_S \sigma \sqrt{\pi}}{\delta_{g2}} \mathrm{e}^{\frac{\sigma^2 - 4\delta_{g2} d_g}{4\delta_{g2}^2}} \mathrm{e}^{-\frac{d_f}{\delta_{f2}}} 0.96 K_{f2} \\ T_{f3} = \dfrac{T_S \sigma \sqrt{\pi}}{\delta_{g3}} \mathrm{e}^{\frac{\sigma^2 - 4\delta_{g3} d_g}{4\delta_{g3}^2}} \mathrm{e}^{-\frac{d_f}{\delta_{f3}}} 0.96 K_{f3} \\ T_{f4} = \dfrac{T_S \sigma \sqrt{\pi}}{\delta_{g4}} \mathrm{e}^{\frac{\sigma^2 - 4\delta_{g4} d_g}{4\delta_{g4}^2}} \mathrm{e}^{-\frac{d_f}{\delta_{f4}}} 0.96 K_{f4} \end{cases} . \tag{18}$$

Numerical solution of that set of equations makes it possible to determine all parameters of temperature distribution in the examined tissue (T_S, σ, d_g, d_f). Complete depth of the heat source is expressed by the following equation:

$$d = d_g + d_f + d_s \approx d_g + d_f . \tag{19}$$

Because it is relatively easy to estimate the thickness of a fat layer, it is possible to determine temperature distribution using three-band measurement introducing into relation (16) a resultant factor defined by equation:

$$K_{ri} = t_{gfi} \mathrm{e}^{-\frac{d_f}{\delta_{fi}}} K_{fi} . \tag{20}$$

Formula (16) simplifies to

$$T_{fi} = \frac{T_S \sigma \sqrt{\pi}}{\delta_{gi}} \mathrm{e}^{\frac{\sigma^2 - 4\delta_{gi} d_g}{4\delta_{gi}^2}} K_{ri} . \tag{21}$$

As a result of three-band measurement and using formula (21), the following set of equations is obtained:

$$\begin{cases} T_{f1} = \dfrac{T_S \sigma \sqrt{\pi}}{\delta_{g1}} \mathrm{e}^{\frac{\sigma^2 - 4\delta_{g1} d_g}{4\delta_{g1}^2}} K_{r1} \\ T_{f2} = \dfrac{T_S \sigma \sqrt{\pi}}{\delta_{g2}} \mathrm{e}^{\frac{\sigma^2 - 4\delta_{g2} d_g}{4\delta_{g2}^2}} K_{r2} \\ T_{f3} = \dfrac{T_S \sigma \sqrt{\pi}}{\delta_{g3}} \mathrm{e}^{\frac{\sigma^2 - 4\delta_{g3} d_g}{4\delta_{g3}^2}} K_{r3} \end{cases} . \tag{22}$$

By solving above equations, formulas describing real temperature distribution in examined tissue can be written as:

$$d_g = \frac{\alpha \cdot \delta_{g1}^2 (\delta_{g2}^2 - \delta_{g3}^2) - \beta \cdot \delta_{g3}^2 (\delta_{g1}^2 - \delta_{g2}^2)}{\delta_{g1}^2 (\delta_{g2} - \delta_{g3}) - \delta_{g2}^2 (\delta_{g1} - \delta_{g3}) + \delta_{g3}^2 (\delta_{g1} - \delta_{g2})} ,$$

$$\sigma = 2\delta_{g1}\delta_{g2} \sqrt{\frac{d_g (\delta_{g2}^{-1} - \delta_{g1}^{-1}) - \alpha}{\delta_{g1}^2 - \delta_{g2}^2}} ,$$

$$T_S = \frac{T_{f1} \delta_{g1}}{\sigma K_{r1} \sqrt{\pi}} \mathrm{e}^{\frac{4\delta_{g1} d_g - \sigma^2}{4\delta_{g1}^2}} , \tag{23}$$

where:

$$\alpha = \ln \left(\frac{T_{f1} K_{r2} \delta_{g1}}{T_{f2} K_{r1} \delta_{g2}} \right) , \quad \beta = \ln \left(\frac{T_{f2} K_{r3} \delta_{g2}}{T_{f3} K_{r2} \delta_{g3}} \right) .$$

Complete depth of the heat source is increased by width of fat and skin layers and can be calculated using formula (19).

Numerical analysis of formulae shown in this chapter leads to a conclusion that results of estimation of unknown temperature distribution strongly depend on accuracy of T_{fi} temperature measurements. This is a result of rapidly changing exponential functions appearing in final formulae. Therefore it seams reasonable to conduct extra measurements on other frequencies to precise the results. It requires the choice of an optimal algorithm of solving redundant set of nonlinear equations.

4. Experimental results

The setup we used for verification of this method, is presented in Fig. 4. A chunk of beef was used as tissue. We used a poly-propylene tube of diameter 5 mm, containing 1.5% saline solution as the heat source.

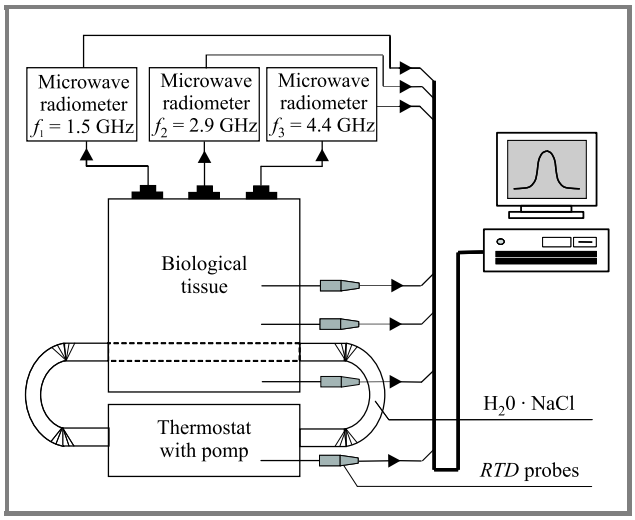

Fig. 4. Scheme of the measurement.

Temperature of solution was regulated by the thermostat. To inspect the physical temperature distribution inside the tissue we used mini hypodermic probes with platinum *RTD* element. In the range of temperatures from 30°C to 45°C, conductivity of the solution is about 2 S/m, and relative permittivity falls into a range from 70 to 75. Such parameters assure very good coefficient of power transmission across the solution – tissue interface, equal to 0.99 for all measurement frequencies. Side of tube can be omitted in analysis because its thickness is only 0.1 mm.

To test the non-invasive thermometry based on the principles described in this paper, we used the experimental three-band radiometer system, which measured temperature brightness at $f_1 = 1.5$ GHz, $f_2 = 2.9$ GHz and $f_3 = 4.4$ GHz. Main parameters of the radiometric measurement system are given in Table 1. Measurements were made automatically and the results were displayed and stored using a PC.

Table 1
Main parameters of the radiometric system

Parameters	f_i [GHz]		
	1.5	2.9	4.4
RF bandwidth, B_{HF} [MHz]	180	390	485
Noise temperature, T_R [K]	215	425	558
Equivalent integrating time [15], $\tau = \dfrac{1}{2B_{LF}}$ [s]	6	6	6
Integration time, t [s]	10	10	10
Resolution*, $\Delta T = 2\dfrac{T_A + T_R}{\sqrt{B_{HF}\tau}}$ [K]	0.032	0.030	0.032
* Brightness temperature resolution (sensitivity) calculated according to [15, 25] for $T_A = 310$ K.			

Radiometer working at the highest frequency determines the overall capability of the measurement system to estimate depth and size of a heat source. It is because high frequency microwaves cannot deeply penetrate tissues. Then again, radiometer working at the lowest frequency determines probability of detection of a heat source in antenna's field of view.

As a result of a calibration process we obtain coefficients: $K_{f1} = 1.05$, $K_{f2} = 1.2$ and $K_{f3} = 0.8$ and power penetration depths for the investigated tissue: $\delta_{m1} = 6.6$ mm, $\delta_{m2} = 3.8$ mm, $\delta_{m3} = 3.0$ mm.

Experiment involved wide distribution of temperature. Distribution should be sufficiently wide in relation to dimensions of tube, so that its influence on results was prevailing.

Figure 5 shows typical results obtained for temperature distribution with the following parameters: $T_S = 20$°C, $d_m = 20$ mm and $\sigma = 6.2$ mm. The result of radiometric measurements, calculated on the basis of Eqs. (14) and (3), is shown as a solid curve and the results of direct measurements by the *RTD* probes are shown as points.

As the brightness temperatures T_{fi} fluctuate randomly due to the nature of thermal radiation, the deep-seated profile of temperature distribution estimated from them also fluctuates randomly. We computed numerically the error in estimating this profile by means of a Monte Carlo technique. We used a 95.5% confidence level to define the accuracy of tissue temperature measurement. It was illustrated by dashed lines in Fig. 5.

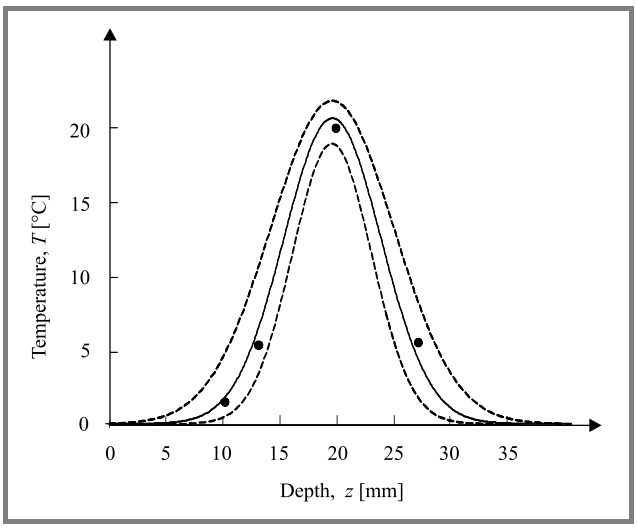

Fig. 5. Results of measurements.

From this chart, we can conclude that the correctness of the presented analysis for single homogenous muscle layer has been confirmed by experiment. Results obtained indicate a possibility of non-invasive detection and measurement of spatial temperature distribution inside a human body by means of multifrequency microwave thermograph.

5. Conclusion

The objective of this article was to present a measurement method suitable to estimate deep-seated temperature distribution by means of a multifrequency microwave thermograph. Theoretical analysis justified initial assumptions, on which the method of estimating temperature distribution inside biological tissues was based. Experimental results confirmed that for single homogenous muscle layer it is possible to estimate the deep-seated profile of temperature distribution after a three-band measurement. For three layers (gland, fat and skin) a multi-band measurement is necessary with four radiometers working at different frequencies. Additional conditions make this measurement possible with only three radiometers.

Considering measurement error, a kind of redundancy in data acquisition is advisable. This makes the whole system less sensitive to random fluctuations of brightness temperatures T_{fi}. Research suggests adding a 5th frequency around 1 GHz (to obtain the deepest penetration) in the radiometer system.

References

[1] F. Bardati, M. Bertero, M. Mongiardo, and D. Solimini, "Singular system analysis of the inversion of microwave radiometric data: applications to biological temperature retrieval", *Inv. Probl.*, vol. 3, pp. 347–370, 1987.

[2] B. Bocquet, J. C. Van De Velde, A. Mamouni, Y. Leroy, G. Giaux, J. Delannoy, and D. Delvalee, "Microwave radiometric imaging at 3 GHz for the exploration of breast tumours", *IEEE Trans. MTT*, vol. 38, no. 6, pp. 791–793, 1990.

[3] D. V. Land, "A clinical microwave thermography system", *IEE Proc.*, vol. 134, no. 2, pp. 193–200, 1987.

[4] Y. Leroy, A. Mamouni, J. C. Van De Velde, B. Bocquet, and B. Dujardin, "Microwave radiometry for non-invasive thermometry", *Automedica*, vol. 8, no. 4, pp. 181–202, 1987.

[5] Y. Leroy, A. Mamouni, J. C. Van De Velde, B. Bocquet, G. Giaux, and J. Dellanoy, "Non-invasive measurement of subcutaneous tissue temperature by microwave radiometry", *Innov. Tech. Biol. Med.*, vol. 12 (special 1), pp. 155–162, 1991.

[6] A. Mamouni, Y. Leroy, B. Bocquet, J. C. Van De Velde, and F. Gelin, "Computation of near – field microwave radiometric signals: definition and experimental verification", *IEEE Trans. MTT*, vol. 39, no. 1, pp. 124–132, 1991.

[7] B. Stec, "Microwave thermography: methods and equipment", in *11th Int. Conf. Microw., Radar Wirel. Commun., Worksh.*, Warsaw, Poland, 1996, pp. 97–114.

[8] F. Sterzer, "Microwave radiometers for non-invasive measurements of subsurface tissue temperatures", *Automedica*, vol. 8, no. 4, pp. 203–211, 1987.

[9] B. Bocquet, P. DeHour, A. Mamouni, J. C. Van De Velde, and Y. Leroy, "Near field microwave radiometric weighting functions for multilayered materials", *J. Electromagnet. Wav. Appl.*, vol. 7, no. 11, pp. 1497–1514, 1993.

[10] L. Dubois, J. Pribetich, J. Falbre, M. Chive, and Y. Moschetto, "Non-invasive microwave multifrequency radiometry used in microwave hyperthermia for bidimensional reconstruction of temperature patterns", *Int. J. Hyperther.*, vol. 9, pp. 415–431, 1993.

[11] K. Maruyma, S. Mizushina, T. Sugiura, G. M. J. Van Leeuwen, J. W. Hand, G. Marrocco, F. Bardati, A. D. Edwards, D. Azzopardi, and D. Land, "Feasibility of non-invasive measurement of deep brain temperature in newborn infants by multifrequency microwave radiometry", *IEEE Trans. MTT*, vol. 48, no. 11, pp. 2141–2147, 2000.

[12] S. Mizushina, T. Shimizu, K. Suzuki, M. Kinomura, H. Ohba, and T. Sugiura, "Retrieval of temperature-depth profiles in biological objects from multifrequency microwave radiometric data", *J. Electromagnet. Wav. Appl.*, vol. 7, no. 11, pp. 1515–1548, 1993.

[13] H. Ohba, M. Kinomura, M. Ito, T. Sugiura, and S. Mizushina, "Multifrequency microwave radiometry for non-invasive thermometry using a new temperature profile model function", in *Asia Pacif. Microw. Conf.*, Tokyo, Japan, 1994, pp. 401–404.

[14] F. Bardati, V. J. Brown, and P. Tognolatti, "Temperature reconstructions in a dielectric cylinder by multifrequency microwave radiometry", *J. Electromagnet. Wav. Appl.*, vol. 7, no. 11, pp. 1549–1571, 1993.

[15] M. E. Tiuri, "Radio astronomy receivers", *IEEE Trans. Antenn. Propag.*, vol. 12, pp. 930–938, 1964.

[16] B. Stec and M. Żurawski, "Compensated microwave thermometer for medical applications", in *Asia Pacif. Microw. Conf.*, Tokyo, Japan, 1994, pp. 405–408.

[17] B. Stec and W. Susek, "A 4.4 GHz microwave thermometer with compensation of reflection coefficient", in *13th Int. Conf. Microw., Radar Wirel. Commun.*, Wrocław, Poland, 2000, pp. 453–456.

[18] B. Stec and A. Dobrowolski, "Estimation of internal distribution of temperature inside biological tissues by means of multifrequency microwave thermograph", in *13th Int. Conf. Microw., Radar Wirel. Commun.*, Wrocław, Poland, 2000, pp. 577–580.

[19] B. Stec and A. Dobrowolski, "Estimation of internal distribution of temperature inside biological tissues by means of multifrequency microwave thermograph", *J. Telecommun. Inform. Technol.*, no. 1, pp. 39–42, 2002.

[20] B. Stec, A. Dobrowolski, and W. Susek, "Estimation of temperature distribution inside biological tissues by means of multifrequency microwave thermograph", in *23rd Ann. Int. Conf. IEEE Eng. Med. Biol. Soc.*, Istanbul, Turkey, 2001.

[21] B. Stec, A. Dobrowolski, and W. Susek, "Estimation of deep-seated profile of temperature distribution inside biological tissues by means of multifrequency microwave thermograph", in *IEEE MTT-S Int. Microw. Symp.*, Seattle, USA, 2002, pp. 2261–2264.

[22] W. Kazanowska, P. Knapp, A. Mazurek, T. Filipkowski, and B. Stec, "An attempt to employ microwave thermography for the evaluation of potential danger of breast cancer", in *8th Int. Meet. Gynaecol. Oncol.*, Barcelona, Spain, 1993.

[23] T. Maeda, "Diagnosis of mammary gland diseases using microwave thermography: a study on adjunctive diagnostic methods in relation to different factors in breast diseases", *Nippon-Geka-Gakkai-Zasshi*, vol. 91, no. 5, pp. 622–630, 1990.

[24] M. A. Stuchly and S. S. Stuchly, "Dielectric properties of biological substances – tabulated", *J. Microw. Pow.*, vol. 15, no. 1, pp. 19–26, 1980.

[25] D. F. Wait, "The sensitivity of the Dicke radiometer", *J. Res. Natl. Bur. Stand. – C. Eng. Instrum.*, vol. 71C, no. 2, 1967.

Bronisław Stec – for biography, see this issue, p. 115.

Andrzej Dobrowolski, **Waldemar Susek** – for biography, see this issue, p. 116.